Title: Non-linear Growth Kinetics of Breast Cancer Stem Cells: Implications for Cancer Stem Cell Targeted Therapy

Authors: Xinfeng Liu, Sara Johnson, Shou Liu, Deepak Kanojia, Wei Yue, Udai Singn, Qian Wang, Qi Wang, Qing Nie, and Hexin Chen

Supplementary Data

Supplementary Methods

Western Blot analysis. Protein concentration was measured using BCA kit (Thermo Scientific, Rockford, IL, USA) and protein lysates were separated by SDS-PAGE and then blotted onto Hybond-C extra membranes (GE Healthcare, Buckinghamshire, UK) for Western blot analysis. Antigen-antibody reaction was detected using Super Signal West Pico and Femto chemiluminescent substrate kits according to manufacturer's instructions (Thermo Scientific). The primary antibodies used for Western blot analysis are purchased from Cell Signaling Technology (Beverly, MA).

Supplementary Results and Discussion

A simple cell lineage model without feedback control

We assume that the breast cancer cells can approximately be divided into three main types in our model: cancer stem cells (CSCs), progenitor cells (PCs), and terminally differentiated cells (TDCs). We denote $x_i(t)$ the number of cells at time *t* for cell type *i*, *i=0,1,2*, p_0 the probability that a CSC is divided into a pair of CSCs, q_0 the probability that a CSC is divided into a pair of PCs, p_1 the probability that a PC is divided into a pair of PCs, and q_1 the probability that a PC is divided into a pair of TDCs, respectively. Thus, $1-p_0-q_0(1-p_1-q_1)$ denotes the probability that an asymmetric cell division takes place from CSCs (PCs) to PCs (TDCs). Dynamics of the cell population consisting of the three cell types, when feedback control is not included, can be described by the following system of ordinary differential equations (ODEs),

$$\begin{aligned}
\frac{dx_0(t)}{dt} &= (p_0-q_0)v_0x_0(t)-d_0x_0(t),\\
\frac{dx_1(t)}{dt} &= (1-p_0+q_0)v_0x_0(t)+(p_1-q_1)v_1x_1(t)-d_1x_1(t),\\
\frac{dx_2(t)}{dt} &= (1-p_1+q_1)v_1x_1(t)-d_2x_2(t).
\end{aligned} \tag{S1}$$

Here v_0 and v_1 are the synthesis rates, which quantify how rapidly cells divide at each lineage stage in unit time, d_i is the degradation rate of CSCs, PCs or TDCs at *i=0,1,2*, respectively, where the degradation rates for CSCs and PCs (d_0 and d_1) should be relatively small or negligible compared to that of TDCs. To reach a non-zero steady-state, $d_0 = (p_0 - q_0)v_0$ and $d_1 < (p_1 - q_1)v_1$. When $d_0 = (p_0 - q_0)v_0$, the population of CSCs ($x_0(t)$) keeps a constant for all time. With zero initial states for both PCs and TDCs, the solutions for the cell populations of PCs and TDCs are given by

$$x_1(t) = \frac{(1 - p_0 + q_0)v_0 x_0}{d_1 - (p_1 - q_1)v_1}\left(1 - e^{((p_1 - q_1)v_1 - d_1)t}\right),$$

$$x_2(t) = \frac{(1 - p_0 + q_0)(1 - p_1 + q_1)v_0 v_1 x_0}{d_1 - (p_1 - q_1)v_1} \times$$

$$\left(\frac{1}{d_2} + \left(\frac{1}{(p_1 - q_1)v_1 - d_1 + d_2} - \frac{1}{d_2}\right)e^{-d_2 t} - \frac{e^{((p_1 - q_1)v_1 - d_1)t}}{(p_1 - q_1)v_1 - d_1 + d_2}\right).$$

At steady states, in particular,

$$x_1(t) = \frac{(1 - p_0 + q_0)v_0 x_0}{d_1 - (p_1 - q_1)v_1}, \quad x_2(t) = \frac{(1 - p_0 + q_0)(1 - p_1 + q_1)v_0 v_1 x_0}{(d_1 - (p_1 - q_1)v_1)d_2}.$$

Mathematical models with negative feedback regulations

Since stem cells can regulate its population through their cell division and other mechanisms, a feedback mechanism is a viable way to self-regulate their populations. One feedback mechanism is to assume the TDCs can regulate the synthesis rates of CSCs and PCs, known as Type I feedback. When the synthesis rate, the *v*-parameter, is regulated by the negative feedback from TDCs by Hill functions with a Hill coefficient of 2 and feedback strength parameters β's with a time delay τ, the equations for the system take the following form,

$$\begin{aligned}
\frac{dx_0(t)}{dt} &= (p_0 - q_0)\frac{v_0}{1 + \beta_0 (x_2(t - \tau))^2}x_0(t) - d_0 x_0(t), \\
\frac{dx_1(t)}{dt} &= (1 - p_0 + q_0)\frac{v_0}{1 + \beta_0 (x_2(t - \tau))^2}x_0(t) + (p_1 - q_1)\frac{v_1}{1 + \beta_1 (x_2(t - \tau))^2}x_1(t) - d_1 x_1(t), \quad \text{(S2)} \\
\frac{dx_2(t)}{dt} &= (1 - p_1 + q_1)\frac{v_1}{1 + \beta_1 (x_2(t - \tau))^2}x_1(t) - d_2 x_2(t).
\end{aligned}$$

Another feedback mechanism is to assume the probability of symmetric cell division is regulated by the population of TDCs, known as Type-II feedback. When *p*- and *q*-parameters are controlled by the negative feedback again by Hill functions with a Hill coefficient of 2 and feedback strength parameters $\gamma's$ with a time delay τ, the governing equations take the form,

$$\begin{aligned}
\frac{dx_0(t)}{dt} &= \left(\frac{p_0}{1+\gamma_1^0\left(x_2(t-\tau)\right)^2} - \frac{q_0}{1+\gamma_2^0\left(x_2(t-\tau)\right)^2} \right) v_0 x_0(t) - d_0 x_0(t), \\
\frac{dx_1(t)}{dt} &= \left(1 - \frac{p_0}{1+\gamma_1^0\left(x_2(t-\tau)\right)^2} + \frac{q_0}{1+\gamma_2^0\left(x_2(t-\tau)\right)^2} \right) v_0 x_0(t) \\
&\quad + \left(\frac{p_1}{1+\gamma_1^1\left(x_2(t-\tau)\right)^2} - \frac{q_1}{1+\gamma_2^1\left(x_2(t-\tau)\right)^2} \right) v_1 x_1(t) - d_1 x_1(t), \\
\frac{dx_2(t)}{dt} &= \left(1 - \frac{p_1}{1+\gamma_1^1\left(x_2(t-\tau)\right)^2} + \frac{q_1}{1+\gamma_2^1\left(x_2(t-\tau)\right)^2} \right) v_1 x_1(t) - d_2 x_2(t).
\end{aligned} \tag{S3}$$

If we combine both Type I and Type II feedback mechanisms in the model, the governing system of equations takes the form,

$$\begin{aligned}
\frac{dx_0(t)}{dt} &= \left(\frac{p_0}{1+\gamma_1^0\left(x_2(t-\tau)\right)^2} - \frac{q_0}{1+\gamma_2^0\left(x_2(t-\tau)\right)^2} \right) \frac{v_0}{1+\beta_0\left(x_2(t-\tau)\right)^2} x_0(t) - d_0 x_0(t), \\
\frac{dx_1(t)}{dt} &= \left(1 - \frac{p_0}{1+\gamma_1^0\left(x_2(t-\tau)\right)^2} + \frac{q_0}{1+\gamma_2^0\left(x_2(t-\tau)\right)^2} \right) \frac{v_0}{1+\beta_0\left(x_2(t-\tau)\right)^2} x_0(t) \\
&\quad + \left(\frac{p_1}{1+\gamma_1^1\left(x_2(t-\tau)\right)^2} - \frac{q_1}{1+\gamma_2^1\left(x_2(t-\tau)\right)^2} \right) \frac{v_1}{1+\beta_1\left(x_2(t-\tau)\right)^2} x_1(t) - d_1 x_1(t), \\
\frac{dx_2(t)}{dt} &= \left(1 - \frac{p_1}{1+\gamma_1^1\left(x_2(t-\tau)\right)^2} + \frac{q_1}{1+\gamma_2^1\left(x_2(t-\tau)\right)^2} \right) \frac{v_1}{1+\beta_1\left(x_2(t-\tau)\right)^2} x_1(t) - d_2 x_2(t).
\end{aligned} \tag{S4}$$

Mathematical modeling for the inter-transition between CSCs and non-stem cancer cells

In comparison with the models with negative feedbacks, another alternative mechanism has been proposed to explain the equilibrium between CSCs and non-stem cancer cells due to the inter-transition of cancer cell populations [1]. In favor of this idea, several studies have shown that CSCs can be generated from non-stem cancer cells [2,3]. We also test the possibility of such a mechanism for the model without feedback control (Fig.

S7A). Our analysis and computation reveals that such a system requires much more strict conditions on the choice of parameters than the one with the two feedback loops in order for the cell population to achieve an equilibrium, and in particular, it fails to match the observed data for the dynamics of fluctuation of CSC contents as well as cell population during the culture course (Fig. S6b & c).

For the system when stem cells can be generated from non-stem cells, the model without feedback regulations can be modified as follows however (here assuming zero death rates for both CSCs and PCs),

$$\begin{aligned}
\frac{dx_0(t)}{dt} &= (p_0 - q_0)\nu_0 x_0(t) + k_0 x_1(t), \\
\frac{dx_1(t)}{dt} &= (1 - p_0 + q_0)\nu_0 x_0(t) + (p_1 - q_1)\nu_1 x_1(t) - k_0 x_1(t) + k_1 x_2(t), \\
\frac{dx_2(t)}{dt} &= (1 - p_1 + q_1)\nu_1 x_1(t) - (d + k_1) x_2(t),
\end{aligned} \tag{S5}$$

where k_i depicts the synthesis rate from cell type i+1 to type i. In order for such a system to reach a non-zero equilibrium state, the following constraints on the parameters need to be held,

$$p_0 < q_0,\ p_1 < q_1,\ \frac{k_0}{q_0 - p_0} + \frac{k_1 + (1 - k_1)(p_1 - q_1)}{d + k_1}\nu_1 = 0. \tag{S6}$$

Even though this system has a potential to reach an equilibrium state, such an equilibrium is very sensitive to the choice of parameter values. In general when k_1 / d is very small, p_1 / q_1 needs to be very close to 1 in order to achieve an equilibrium. Moreover, it is very difficult to match the model predictions with our experimental observations (Fig. S7b & c).

Analysis of tumor sphere formation

In literature [4,5], it is believed that tumorspheres can be derived from either CSCs or PCs. However, the ability of non-stem cells to produce tumorspheres over an extended period of time is quite limited. Therefore, when simulating tumorsphere formation, we add a degradation rate to the equation for progenitor cells (PCs) in our mathematical model with two negative feedback loops. Consequentially, in order to incorporate the observed data into our simulation, we make the following assumptions for continuously passaged tumorspheres: the fraction of tumorspheres which are derived from CSCs is 1:r, and CSCs renew itself N times during sphere formation, and the average cell number for each tumorsphere derived from CSCs is N_c, and the average cell number for each tumorsphere

derived from PCs is N_p. With these assumptions, the frequency of CSCs after one passage is obtained as $2^N/\left(N_c+\left(r-1\right)N_p\right)$. For instance, in order to enrich CSCs with the original proportion of 1%, and using the parameter values from the best estimate of previous observations, $N_c=N_p\approx 300,\ N=6$, and the fraction of tumorspheres derived from CSCs and from PCs ($1{:}r$) needs to be maintained above 1:20.

Direct comparison of mathematical models with/without progenitor cells (PCs) or asymmetric division

A similar model with two negative feedback loops while neglecting asymmetric division and PCs was proposed by Rodriguez-Brenes et al in [6] (here assuming zero death rates for CSCs without time delay), which takes the following form,

$$\begin{aligned}\frac{dx_0(t)}{dt}&=\left(2p_0\left(x_2(t)\right)-1\right)v_0\left(x_2(t)\right)x_0(t),\\ \frac{dx_2(t)}{dt}&=2\left(1-p_0\left(x_2(t)\right)\right)v_0\left(x_2(t)\right)x_0(t)-d_2x_2(t).\end{aligned} \tag{S7}$$

Through steady state analysis as discussed in [6], the system admits one unique non-trivial steady-state solution ($\hat{x}_0,\hat{x}_2$), which is given by,

$$p_0\left(\hat{x}_2\right)=\frac{1}{2},\ \hat{x}_0=\frac{d_2\hat{x}_2}{v_0\left(\hat{x}_2\right)}. \tag{S7a}$$

The sufficient and necessary condition for this steady-state solution to be stable is as follows,

$$-d_2\left(2p_0'\left(\hat{x}_2\right)\hat{x}_2+1\right)+v_0'\left(\hat{x}_2\right)\hat{x}_0<0.$$

A sufficient condition can be taken as,

$$-p_0'\left(\hat{x}_2\right)<\frac{1}{2\hat{x}_2}. \tag{S7b}$$

For the system with the asymmetric division while still neglecting PCs, one way to add negative feedback is on the asymmetric division probability. As reported in [6] and confirmed by our analysis, the addition of negative feedback on the asymmetric division probability itself does not change any of the results from Eq. (S7). Here we implement the negative feedback on q_0 instead, the system of equations then takes the following form,

$$\frac{dx_0(t)}{dt} = \left(p_0\left(x_2(t)\right) - q_0\left(x_2(t)\right)\right) v_0\left(x_2(t)\right) x_0(t),$$
$$\frac{dx_2(t)}{dt} = \left(1 - p_0\left(x_2(t)\right) + q_0\left(x_2(t)\right)\right) v_0\left(x_2(t)\right) x_0(t) - d_2 x_2(t). \quad \text{(S8)}$$

The non-trivial steady-state solution of Eq. (S8) can be found by solving the following equations,

$$p_0\left(\hat{x}_2\right) = q_0\left(\hat{x}_2\right),\ \hat{x}_0 = \frac{d_2 \hat{x}_2}{v_0\left(\hat{x}_2\right)}. \quad \text{(S8a)}$$

For the stationary solution to be asymptotically stable, the necessary and sufficient condition will be,

$$-d_2\left(\left(p_0'\left(\hat{x}_2\right) - q_0'\left(\hat{x}_2\right)\right)\hat{x}_2 + 1\right) + v_0'\left(\hat{x}_2\right)\hat{x}_0 < 0.$$

A sufficient condition can be taken,

$$q_0'\left(\hat{x}_2\right) - p_0'\left(\hat{x}_2\right) < \frac{1}{\hat{x}_2}. \quad \text{(S8b)}$$

For the system with two negative feedbacks while neglecting asymmetric division for both CSCs or PCs (Fig. S5A), the equations take the form,

$$\frac{dx_0(t)}{dt} = \left(2\frac{p_0}{1+\gamma_0\left(x_2(t)\right)^2} - 1\right)\frac{v_0}{1+\beta_0\left(x_2(t)\right)^2} x_0(t) - d_0 x_0(t),$$
$$\frac{dx_1(t)}{dt} = 2\left(1 - \frac{p_0}{1+\gamma_0\left(x_2(t)\right)^2}\right)\frac{v_0}{1+\beta_0\left(x_2(t)\right)^2} x_0(t) + \quad \text{(S9)}$$
$$\left(2\frac{p_1}{1+\gamma_1\left(x_2(t)\right)^2} - 1\right)\frac{v_1}{1+\beta_1\left(x_2(t)\right)^2} x_1(t) - d_1 x_1(t),$$
$$\frac{dx_2(t)}{dt} = 2\left(1 - \frac{p_1}{1+\gamma_1\left(x_2(t)\right)^2}\right)\frac{v_1}{1+\beta_1\left(x_2(t)\right)^2} x_1(t) - d_2 x_2(t).$$

Remarks

1: Mathematical analysis confirmed by computation reveals that the negative feedback on q_0 is crucial for the robust and faithful data fitting.

If a negative feedback is added on the symmetric division probability q_0 or CSCs to produce two PCs instead of asymmetric division probability itself, the condition to control the cell growth becomes more flexible. For instance, the condition in Eq. (S8b) suggests that the negative feedback strengths of q_0 and p_0 can be modulated coordinately to reach a stable stationary point, while the condition in Eq. (S7b) only has one function p_0 to adjust to control the cell growth.

2: Our studies show that the negative feedback on q_0 is crucial in order to simultaneously match two experimental data sets: the overall tumor growth and the relative proportion of CSCs (Figs. 1,2 and S5).

Without asymmetric division, neither the model in Eq. (S7) or model in Eq. (S9) is able to simultaneously match both the overall tumor growth and the relative proportion of CSCs obtained from our experiments (Fig. S5). Both the models in Eq. (S4) and Eq. (S8) with negative feedback regulation on q_0 however can achieve a good agreement with experiments on overall tumor growth as well as relative proportion of CSCs (Figs. 1, 2 and S5). This indicates the importance in designing the appropriate feedback control mechanism in the model.

3: The presence of progenitor cells (PCs) plays an essential role in predicting the roles of overexpression of the oncogene Her2 in breast cancer. From our new experiments, we observe that overexpression of HER2 in MCF7 breast cancer cells has no effect on the growth kinetics of the total cell population (Fig. 3c) even though it results in an almost 13-fold increase in the $CD44^+CD24^-$ cell population (11.4 ± 1.5% vs. 0.9 ± 0.3%) (Fig. 3d).

By neglecting progenitor cells while retaining negative feedback on q_0 like in our model, the model in Eq. (S8) predicts that the increase of symmetric division rate (p_0) by 50% leads to an increase in the percentage of CSCs and it also drastically affects the overall tumor growth. In contrast, the increase in the synthesis rate (v_0) only shifts the curve of the overall tumor growth and the percentage of CSCs to the left without affecting their equilibrium states (Fig. S6). Hence the model in Eq. (S8) is not consistent with our observed data on overexpression of HER2, and thus cannot be used to make a prediction on the role of HER2 in breast cancer.

For our model with PCs included (Eq. (S4)), the growth curves agree with each other within 5% error tolerance even with 50% increased values of p_0, v_0, while the increase of p_0, v_0 dramatically changes the proportion of CSCs (Fig. 3b & c). This is consistent with

the observed data on overexpression of HER2, indicating that it is likely that overexpression of HER2 increases v_0 and/or p_0.

4: The presence of progenitor cells (PCs) is necessary to explain the observed data in tumorsphere culture. As supported in literature [4,5], it is believed that tumorspheres can be derived from either CSCs or PCs.

By neglecting progenitor cells (PCs), neither the model in Eq. (S7) or Eq. (S8) is able to simulate the dynamics of tumorsphere forming capability and relative proportion of CSCs. Assuming that all the tumorsphere arise from CSCs, the tumor spheres for each passage based on the models in Eq. (S7) and (S8) should be identical to each other. Hence the tumor sphere forming capability and the proportion of CSCs in the generation of tumorspheres should always remain with a fixed constant with continuous tumorsphere culture (Fig. S8).

Our analysis and computation based on our model in (S4) suggests that even though the proportion of CSCs shows a sharp increase in the first generation of tumorspheres, it cannot continue to increase over the tumorsphere passages. We test this prediction by evaluating the tumorigenicity of tumorspheric cells at different passages in **syngeneic animals**. We indeed observe that the proportion of CSCs in the first generation of tumorspheres is enriched about 30–fold, however, the tumorigenicity of tumorspheres decreases gradually with continuous tumorsphere culture (Fig. 4).

Supplementary References

1 Gupta, P. B. *et al.* Stochastic state transitions give rise to phenotypic equilibrium in populations of cancer cells. *Cell* **146**, 633-644 (2011).

2 Mani, S. A. *et al.* The epithelial-mesenchymal transition generates cells with properties of stem cells. *Cell* **133**, 704-715 (2008).

3 Iliopoulos, D., Hirsch, H. A., Wang, G. & Struhl, K. Inducible formation of breast cancer stem cells and their dynamic equilibrium with non-stem cancer cells via IL6 secretion. *Proc Natl Acad Sci U S A* **108**, 1397-1402 (2011).

4 Deleyrolle, L. P. *et al.* Determination of somatic and cancer stem cell self-renewing symmetric division rate using sphere assays. *PLoS ONE* **6**, e15844 (2011).

5 Reynolds, B. A. & Rietze, R. L. Neural stem cells and neurospheres--re-evaluating the relationship. *Nature methods* **2**, 333-336 (2005).

6 Rodriguez-Brenes, I. A., Komarova, N. L. & Wodarz, D. Evolutionary dynamics of feedback escape and the development of stem-cell-driven cancers. *Proc Natl Acad Sci U S A* **108**, 18983-18988 (2011).

7 Jenndahl, L. E., Isakson, P. & Baeckstrom, D. c-erbB2-induced epithelial-mesenchymal transition in mammary epithelial cells is suppressed by cell-cell contact and initiated prior to E-cadherin downregulation. *International journal of oncology* **27**, 439-448 (2005).

8 Jenndahl, L. E., Taylor-Papadimitriou, J. & Baeckstrom, D. Characterization of integrin and anchorage dependence in mammary epithelial cells following c-erbB2-induced epithelial-mesenchymal transition. *Tumour Biol.* **27**, 50-58, doi:10.1159/000090156 (2006).

Supplementary Figure Legends

Fig. S1. Comparison of different models. A typical simulation on the overall tumor growth (a) with constant CSC and PC death rates, and (**b**) assuming dependence of CSC and PC death rates on the fraction TDCs. (**c**) Comparison of two plots of y=f(x) with Hill function and exponential form. (**d**) A typical simulation on the overall tumor growth curve with Hill function and exponential form shown in (c) to model negative feedback strength. (**e**) Comparison of two plots of y=f(x) with Hill function and exponential form. (**f**) A typical simulation on the overall tumor growth curve with Hill function and exponential form shown in (e) to model negative feedback strength.

Fig. S2. Dynamic changes in the CD44+/CD24- population over the time course of cell culture. (a). 1 x 10^5 MCF7 cells were seeded onto 10-cm plates every two days from a semi-confluent starting plate. Culture medium was replaced every three days. At certain time, cells were harvested for FACS analysis using FITC-conjugated CD44 and PE-conjugated CD24 antibodies (BD sciences, CA). The experiments were performed in duplicate twice. The average data with standard deviation is shown in the figure. (**b**). FACS sorting out the $CD44^{+}CD24^{-}$ population from MCF7/HER2 cells.

Fig. S3. Morphological analysis and molecular characterization of HER2-overexpressed breast cancer cells and control cells. (a) Mesenchymal cell-like morphological changes in HER2-overexpressing MCF7 cells. Several studies have shown that overexpression of HER2 induces a slow EMT process [7,8]. MCF7/HER2 cells have shown a relatively loose cell-cell contact and a slightly more elongated morphology compared to the control cells. **(b)** Western blot analysis of HER2 signaling pathways.

Fig. S4. Simulated tumor responses to strong anti-cancer drug treatments. (a) Simulated tumor size changes with two different treatments: CSC-targeted therapy, and its combination with conventional chemotherapy. (b) Simulated proportion changes of CSCs with these two different treatment strategies.

Fig. S5. A model without the asymmetric division. (a) Cartoon of a model with two negative feedback loops without asymmetric division. (b) A typical simulation with the best fitting parameters on the dynamics of the total cell number and (c) proportion of CSCs. The estimated parameter values for the simulations are given by: $p_0 = 0.55,\ d_2 / v_0 = 0.01,\ \gamma_1^0 = 2.3 \times 10^{-17},\ \beta_0 = 10^{-13}.$

Fig. S6. A model neglecting PCs with asymmetric division included. (a) Cartoon of a model with two feedback loops assuming two types of cells: CSCs and TDCs. (b) A typical original simulation with the best fitting parameters on the overall tumor growth; and (C) the proportion of CSCs. The comparison to the increase of the symmetric division rate (p_0) and the synthesis rate (v_0) is also shown. The estimated parameter

values for the simulations are given by: $p_0 = 0.51,\ q_0 = 0.19, d_2 / v_0 = 0.01,$ $\gamma_1^0 = 2.4 \times 10^{-17},\ \gamma_2^0 = 1.2 \times 10^{-16},\ \beta_0 = 1.1 \times 10^{-13}.$

Fig. S7. A model for CSCs arising from Non-stem cancer cells. (a) Cartoon of a model for CSCs arising from non-stem cancer cells and their proliferative kinetics. (b) A typical simulation on the total cell number which fails to match the observed data; and (C) the proportion of CSCs is kept at a fixed level for all time, and the constant rate for proportion of CSCs is consistent with the findings in the literature.

Fig. S8. Simulated tumorspheres and frequency of CSCs using the model (S7) without PCs. (a) Simulated number of continuously passaged tumorspheres using the model (S7). The simulation cannot match the experimental observation. (b) Simulated frequency of CSCs during the passages for tumorsphere formation. The model (S7) predicts a fixed constant rate, which is inconsistent with the observed data.

Table S1. The frequency of CSCs from observed data was calculated using limit dilution calculation to best fit the observed data.

	CSC Frequency (observed)	CSC Frequency (prediction)	Ratio of sphere from CSC vs. PC (prediction)	Frequency of sphere formation (observed)	Frequency of sphere formation (prediction)
Adherent	1/1667	1/1786			
Passage 1	1/50	1/48	1:33	1/50	1/48
Passage 2	1/55	1/56	1:39	1/40	1/39
Passage 3	NA	1/59	1:41	1/30	1/31
Passage 4	NA	1/67	1:46	1/23	1/26
Passage 5	NA	1/77	1:53	1/30	1/29
Passage 6	NA	1/91	1:63	1/43	1/47
Passage 7	NA	1/167	1:115	1/17	1/15
Passage 8	1/433	1/500	1:344	1/11	1/13
Passage 9	NA	1/833	1:573	1/8.5	1/11
Passage 10	NA	1/2500	1:1719	1/4.3	1/7
Passage 11	NA	1/6000	1:4125	1/2.9	1/2.3
Passage 12	NA	1/8000	1:5500	1/3.6	1/2.1
Passage 13	1/9000	1/12000	1: 8250	1/2.7	1/2.8

The fraction of CSCs for the first passage was estimated from observed adherent data, from which we calculate CSCs self-renew times during sphere formation for one passage. In all our calculations, we also did not consider the variation in the size of spheres, using the averaged cell number for all spheres in our prediction. NA: not available.

Table S2: (1) Parameters used in Figs. 1C, 2A and 3.

Parameters	No feedback	Type I feedback	Type II feedback	Type I and II feedback
p_0	0.25	0.5	0.5	0.5
q_0	0.2	0.2	0.2	0.2
p_1	0.3	0.5	0.5	0.5
q_1	0.1	0.1	0.1	0.1
v_0 / v_1	0.5	0.5	0.5	0.5
d_2 / v_1	0.05	0.05	0.05	0.05
d_0 / d_2	0.1	0.1	0.1	0.1
d_1 / d_2	0.5	0.5	0.5	0.5
γ_1^0	–	–	5×10^{-14}	10^{-14}
γ_2^0	–	–	7×10^{-15}	10^{-16}
γ_1^1	–	–	6×10^{-13}	10^{-13}
γ_2^1	–	–	2×10^{-15}	10^{-15}
β_0	–	2×10^{-11}	–	8×10^{-12}
β_1	–	3×10^{-12}	–	4×10^{-13}
τ	–	2 (days)	2 (days)	2 (days)

Table S2: (2) Parameters used in Figs. 1D, 2B and 5.

Parameters	Fig. 1D	Fig. 2B	Fig. 5C	Fig. 5D
p_0	0.5	0.5	0.5	0.3
q_0	0.2	0.2	0.2	0.2
p_1	0.5	0.5	0.5	0.5
q_1	0.1	0.1	0.1	0.1
v_0 / v_1	0.5	0.5	0.5	0.5
d_2 / v_1	0.05	0.05	0.15	0.05
d_0 / d_2	0.1	0.1	0.03	0.55
d_1 / d_2	0.5	0.5	0.45	0.63
γ_1^0	10^{-23}	2×10^{-17}	10^{-23}	10^{-23}
γ_2^0	2×10^{-24}	6×10^{-15}	2×10^{-24}	2×10^{-24}
γ_1^1	4×10^{-22}	10^{-15}	4×10^{-22}	4×10^{-22}
γ_2^1	5×10^{-23}	2×10^{-14}	5×10^{-23}	5×10^{-23}
β_0	8×10^{-27}	7×10^{-18}	8×10^{-27}	8×10^{-27}
β_1	4×10^{-27}	3×10^{-18}	4×10^{-27}	4×10^{-27}
τ	2 (days)	2 (days)	2 (days)	2 (days)

All the parameters used in the typical simulations shown in different figures are selected as the same in table (1) only if specified otherwise. For all the tables, the parameters are based on the best fitting from random sampling with L_2 error to the observed temporal dynamic curves. In our computational exploration, we assign each parameter a certain range and randomly select a value lying in this range followed by a normal distribution. For the parameters of *p* and *q*, the constraints that we have considered for the data fitting are $p_0 + p_1 \le 1, q_0 + q_1 \le 1$. From the experimental observation, the self-renewal rates for CSCs should be much slower than that of PCs, and the natural death rates for CSCs and PCs should also be smaller than that of TDCs, which will also be considered for our parameter selection with random sampling. Here for the nature death rates, we assume that $v_0 / v_1 = 0.5,\ d_0 / d_2 = 0.1,\ d_1 / d_2 = 0.5.$ The parameters used in Figs. 5A and 5B are a combination of the ones in Fig. 5C and 5D.

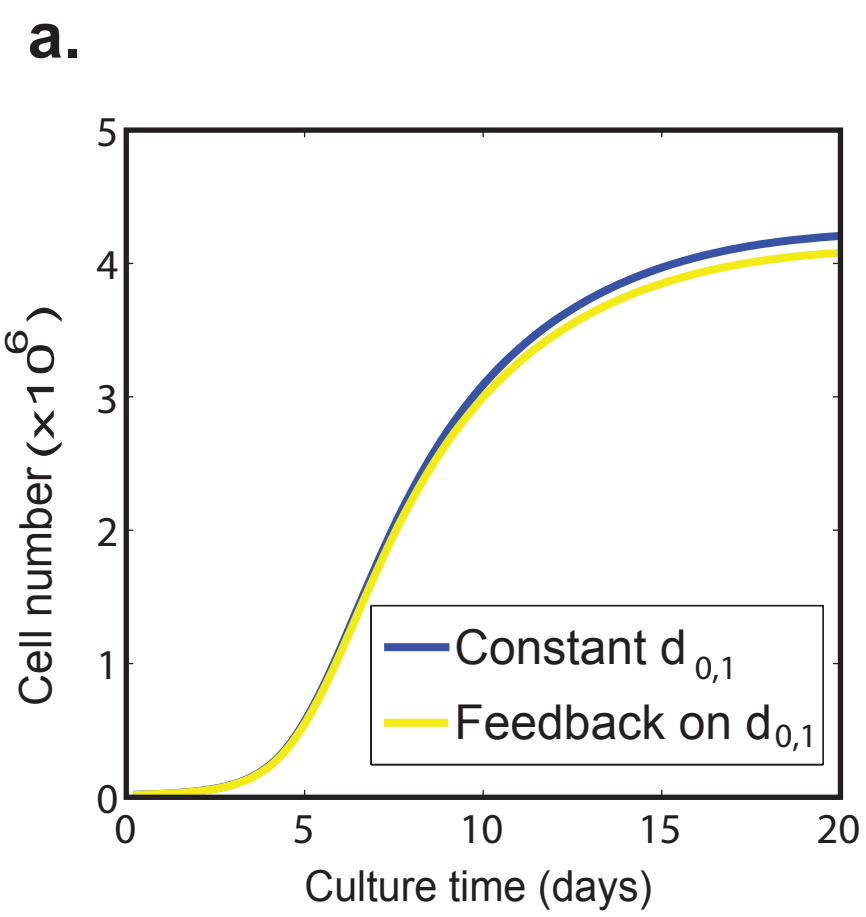
a.
Cell number (x10^6)
Culture time (days)
Constant d 0,1
Feedback on d0,1

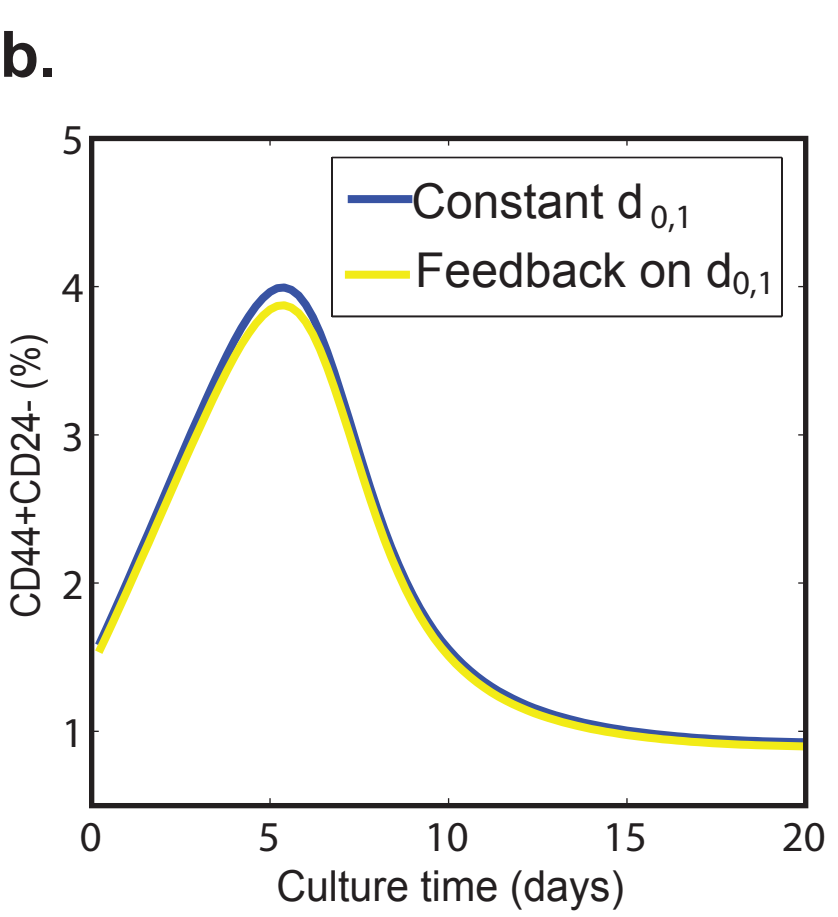
b.
CD44+CD24- (%)
Culture time (days)
Constant d 0,1
Feedback on d0,1

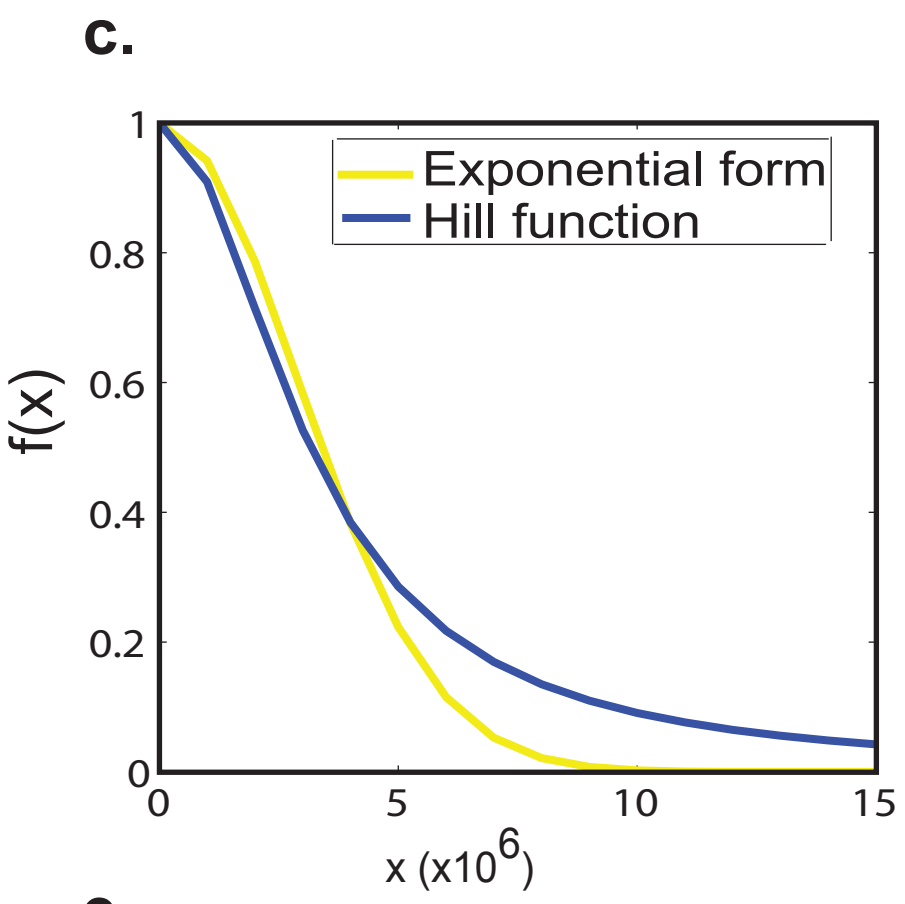
c.
f(x)
x (x10^6)
Exponential form
Hill function

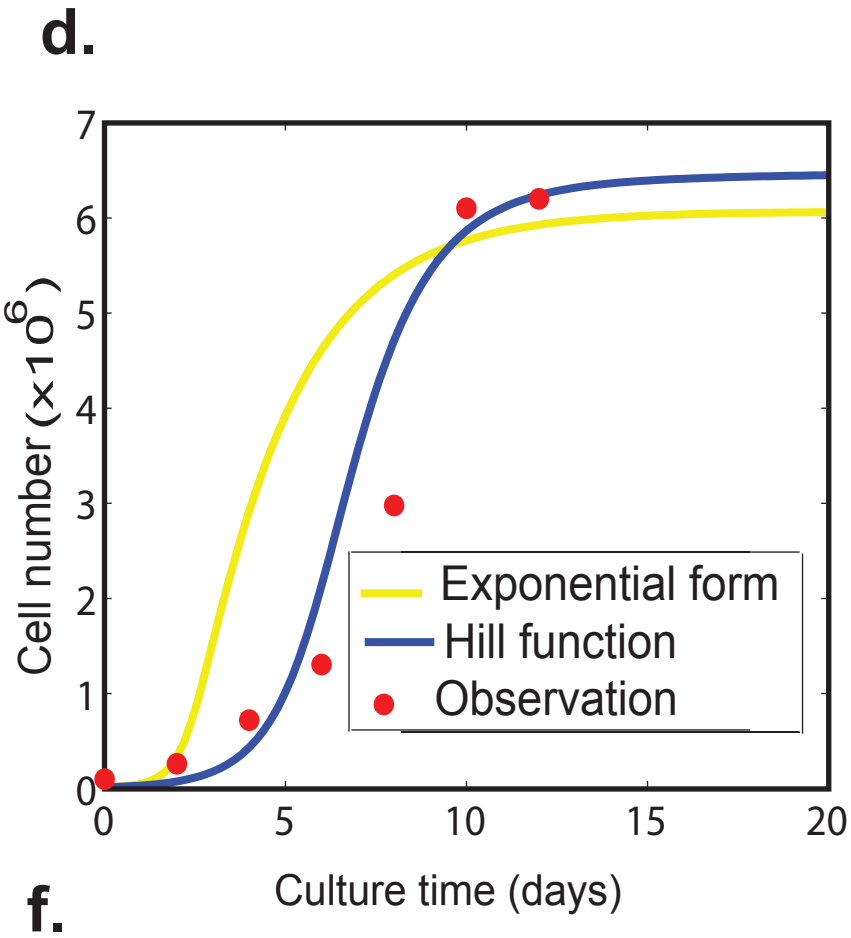
d.
Cell number (x10^6)
Culture time (days)
Exponential form
Hill function
Observation

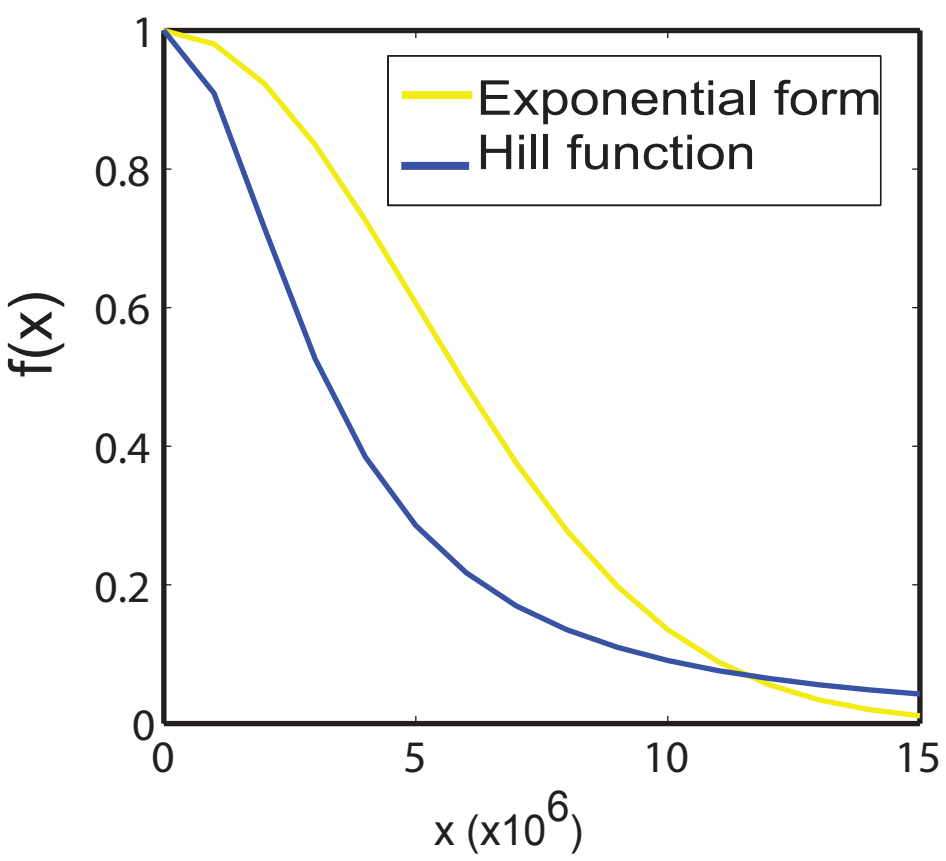
e.
f(x)
x (x10^6)
Exponential form
Hill function

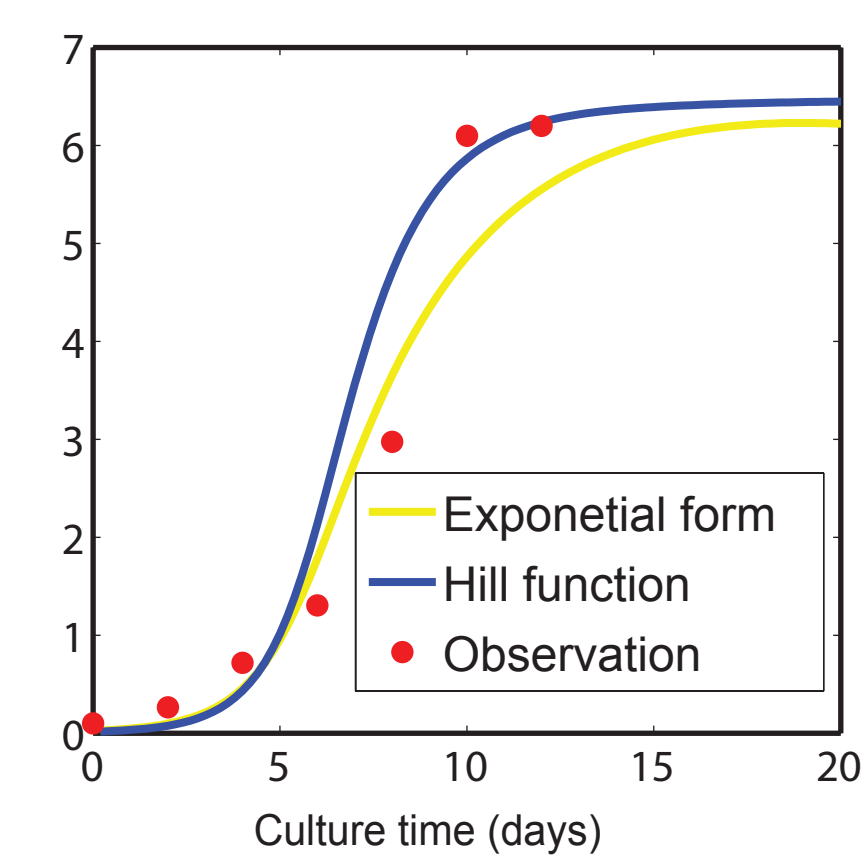
f.
Culture time (days)
Exponetial form
Hill function
Observation

Fig. S1

a.

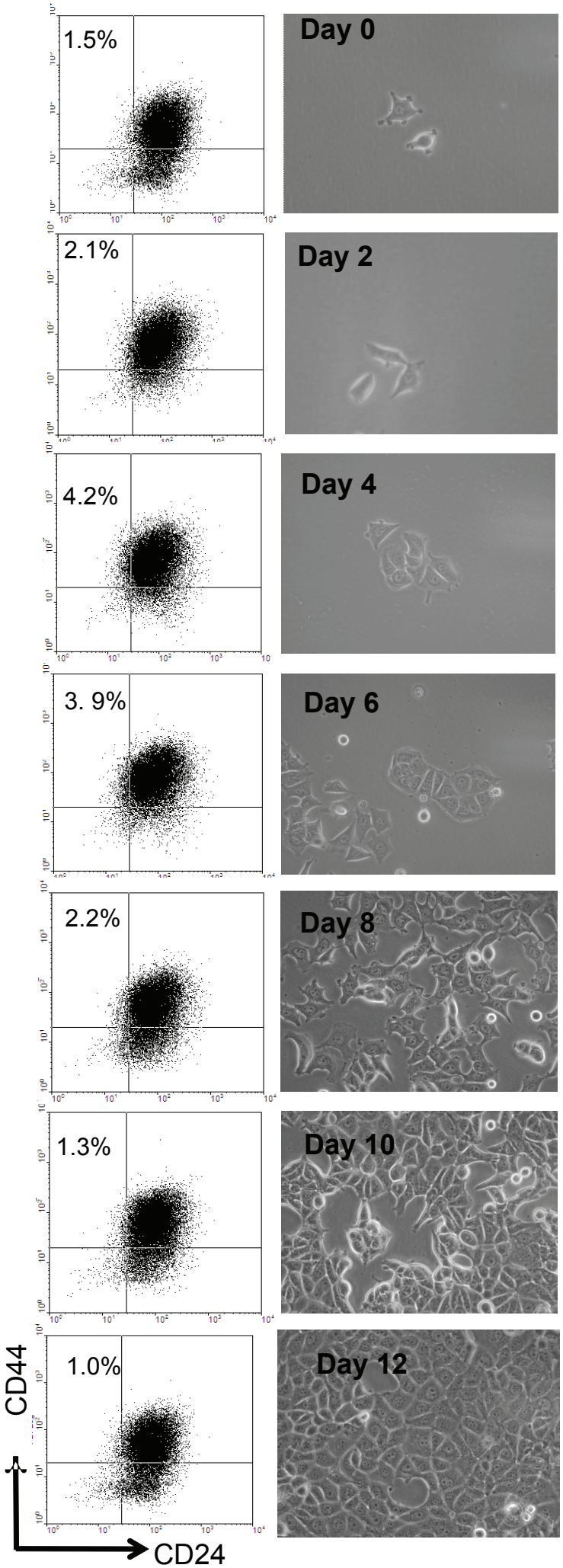
1.5%
Day 0
2.1%
Day 2
4.2%
Day 4
3. 9%
Day 6
2.2%
Day 8
1.3%
Day 10
1.0%
Day 12
CD44
CD24

b.

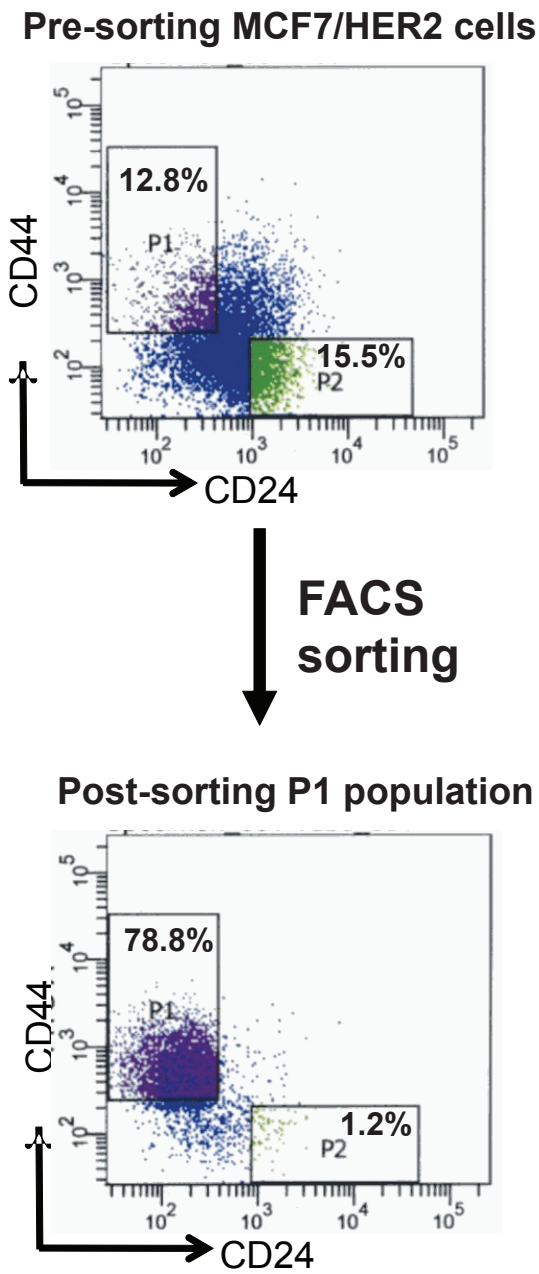
Pre-sorting MCF7/HER2 cells
12.8%
P1
15.5%
P2
CD44
CD24
FACS sorting
Post-sorting P1 population
78.8%
P1
1.2%
P2
CD44
CD24

Fig. S2

a.

MCF7/Neo

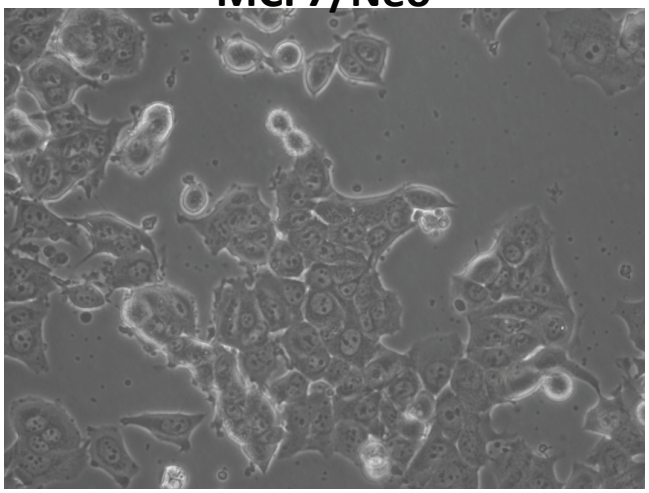

MCF7/HER2

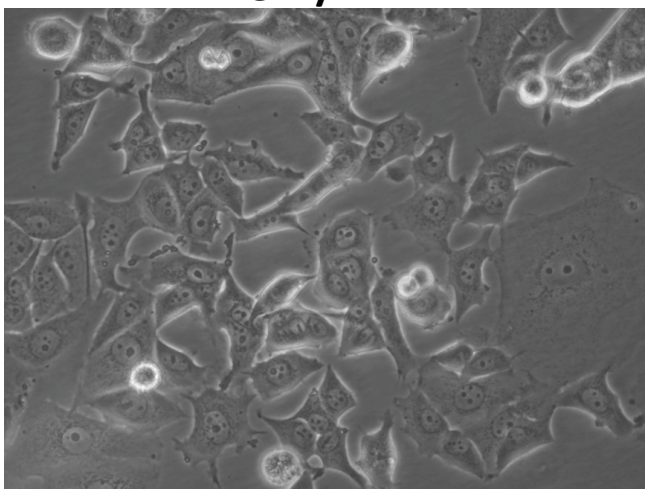

b.

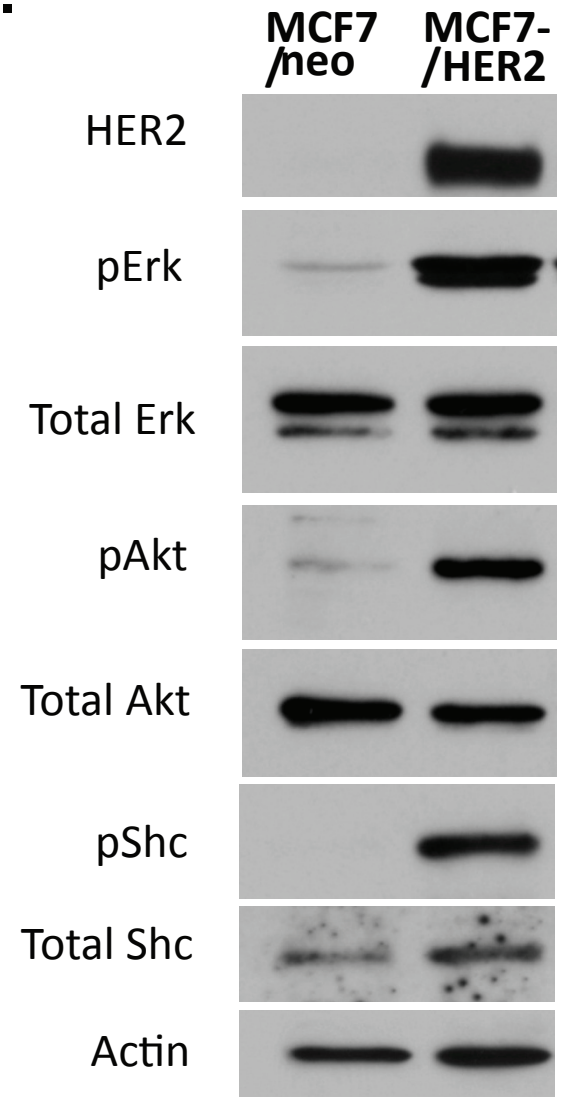

Fig. S3

a.

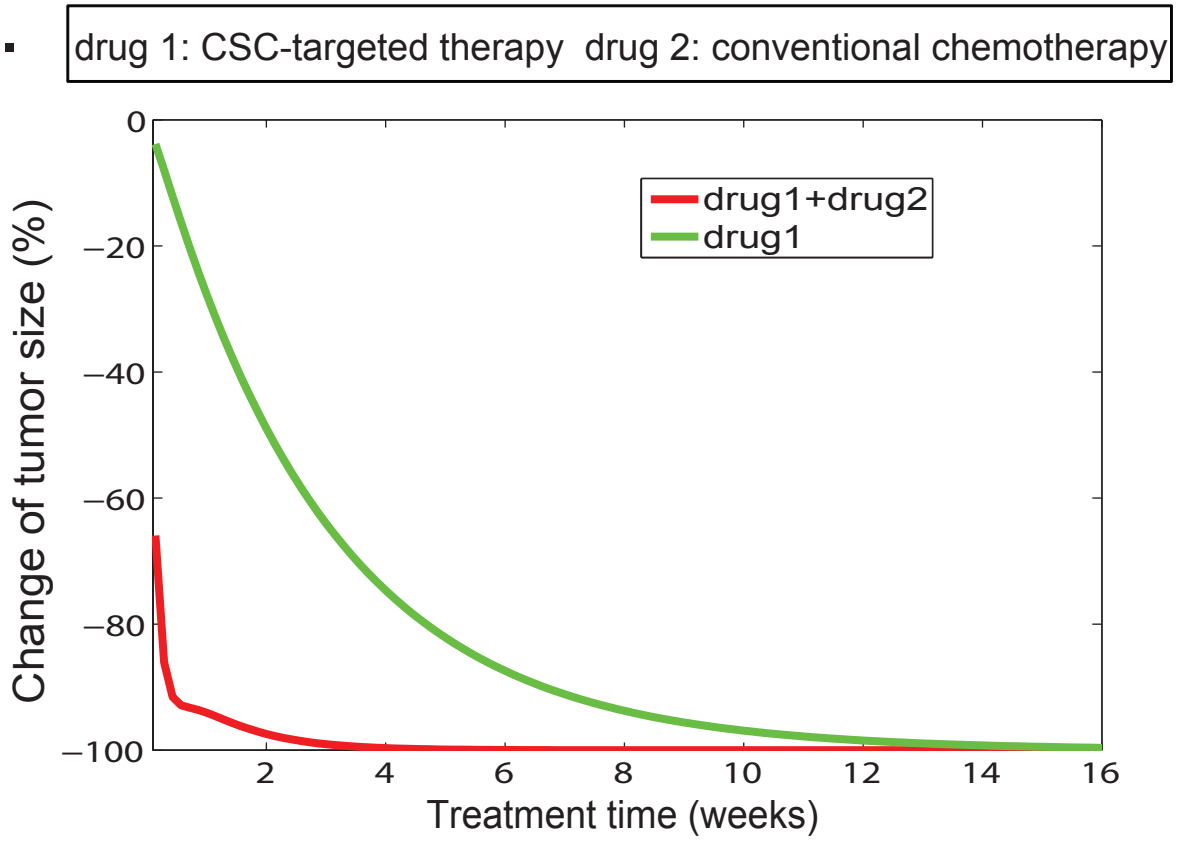
drug 1: CSC-targeted therapy drug 2: conventional chemotherapy
drug1+drug2
drug1
Change of tumor size (%)
0
−20
−40
−60
−80
−100
2
4
6
8
10
12
14
16
Treatment time (weeks)

b.

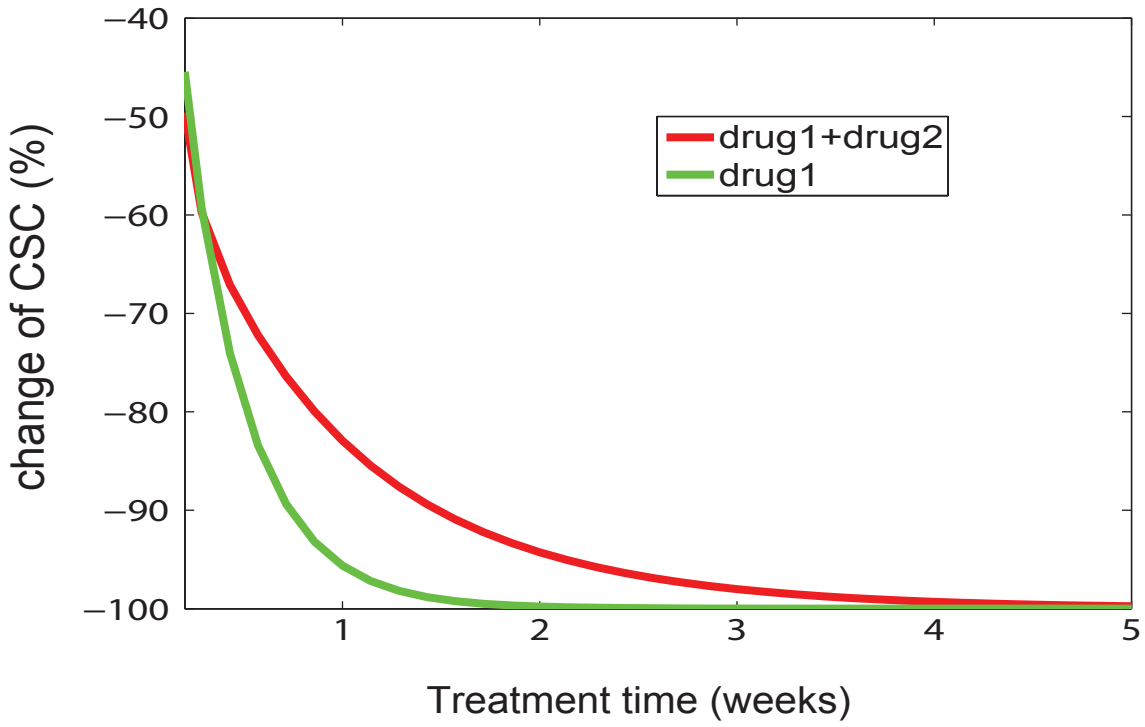
drug1+drug2
drug1
change of CSC (%)
−40
−50
−60
−70
−80
−90
−100
1
2
3
4
5
Treatment time (weeks)

Fig. S4

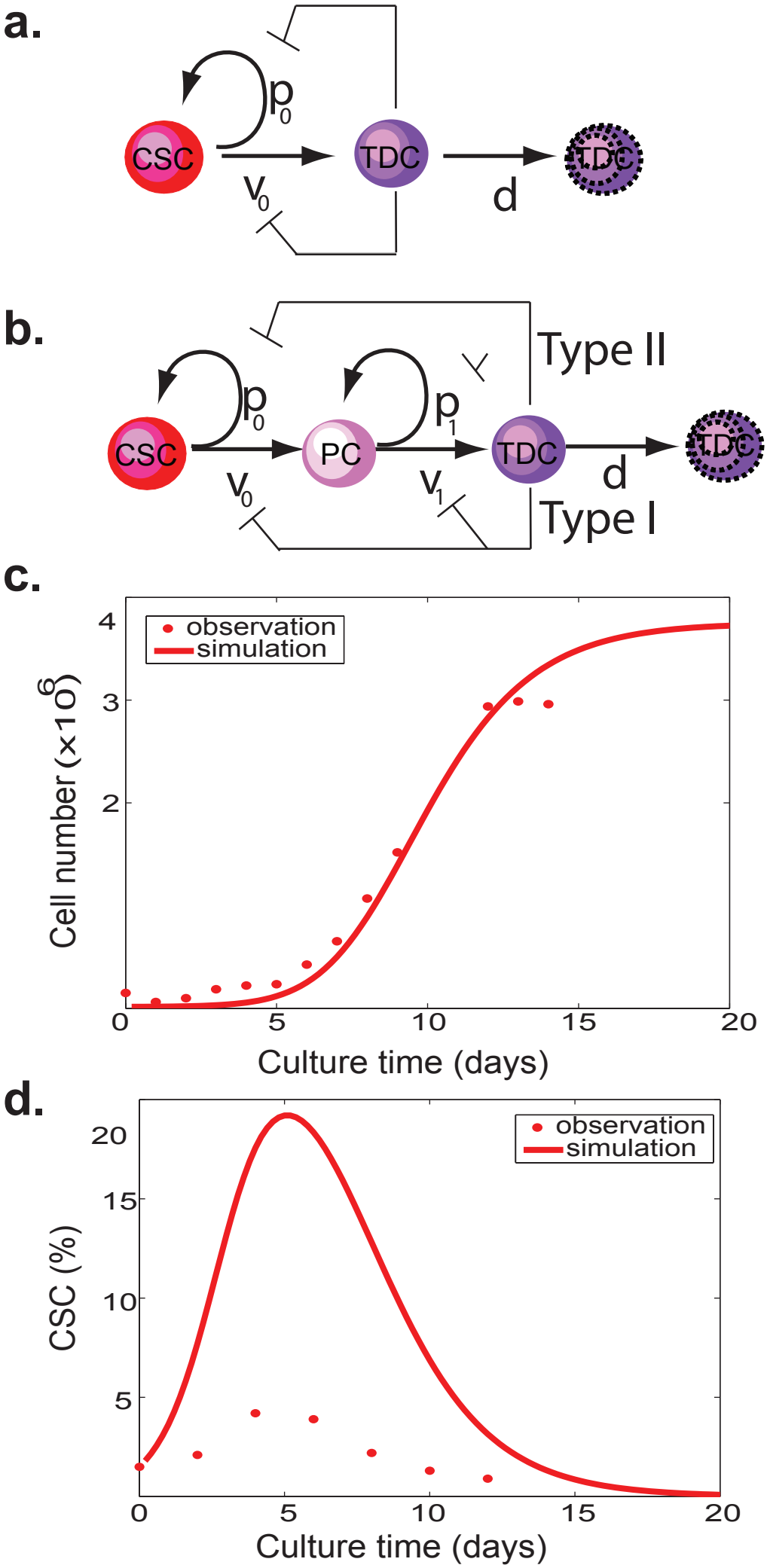
a.
p0
CSC
TDC
TDC
v0
d
b.
Type II
p0
p1
CSC
PC
TDC
TDC
d
v0
v1
Type I
c.
observation
simulation
Cell number (x10^6)
4
3
2
0
5
10
15
20
Culture time (days)
d.
observation
simulation
CSC (%)
20
15
10
5
0
5
10
15
20
Culture time (days)

Fig. S5

a.

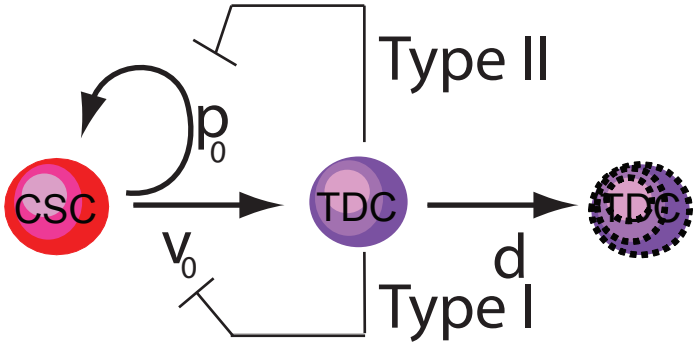
Type II
p0
CSC
TDC
TDC
v0
d
Type I

b.

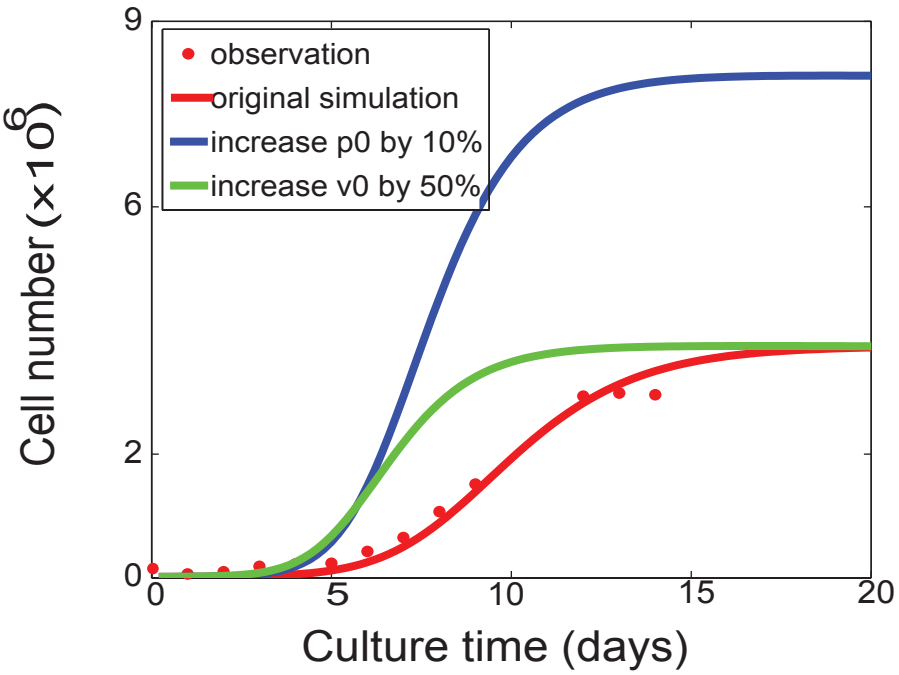
observation
original simulation
increase p0 by 10%
increase v0 by 50%
Cell number (x10^6)
Culture time (days)
0
2
6
9
0
5
10
15
20

c.

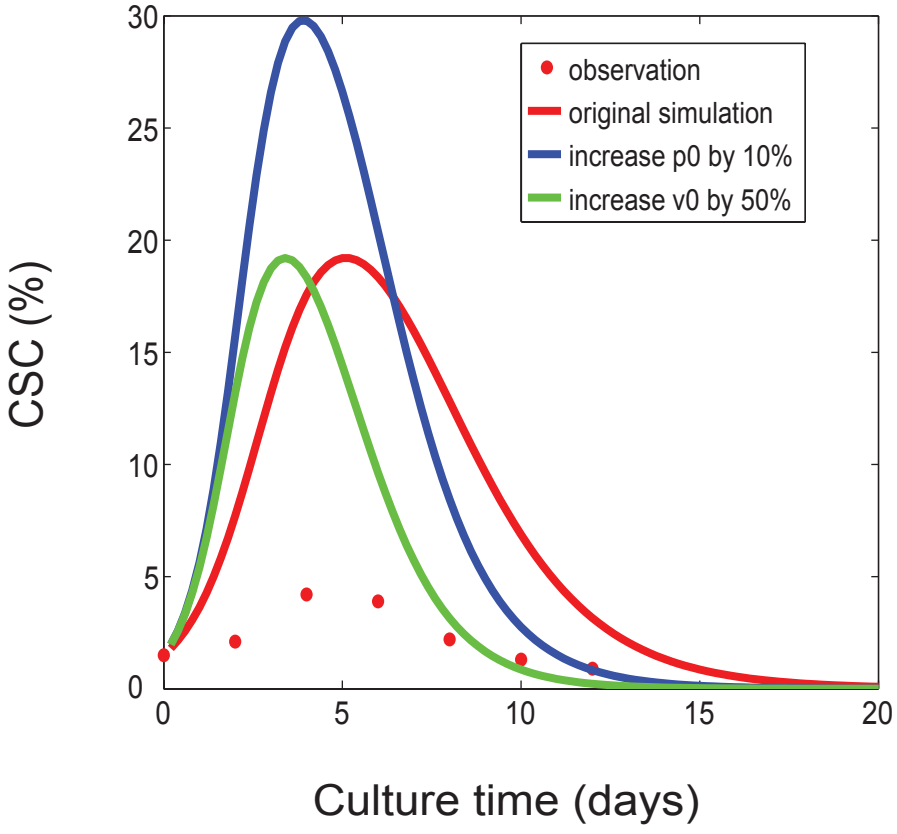
observation
original simulation
increase p0 by 10%
increase v0 by 50%
CSC (%)
Culture time (days)
0
5
10
15
20
25
30
0
5
10
15
20

Fig. S6

a.

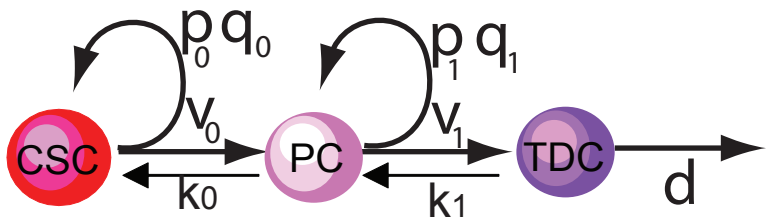
p0 q0
p1 q1
v0
v1
CSC
PC
TDC
k0
k1
d

b.

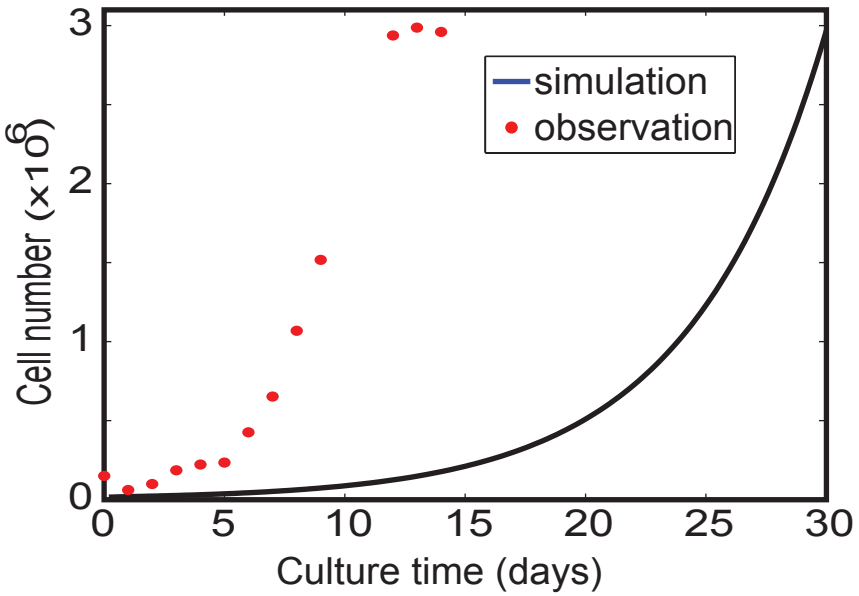
simulation
observation
Cell number (×10^6)
Culture time (days)
0
1
2
3
0
5
10
15
20
25
30

c.

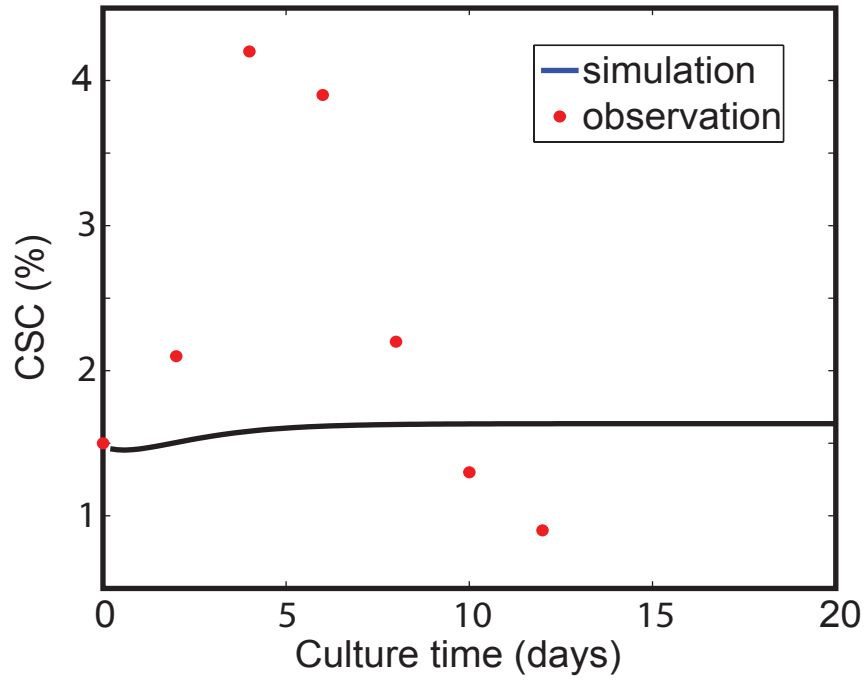
simulation
observation
CSC (%)
Culture time (days)
1
2
3
4
0
5
10
15
20

Fig. S7

a.

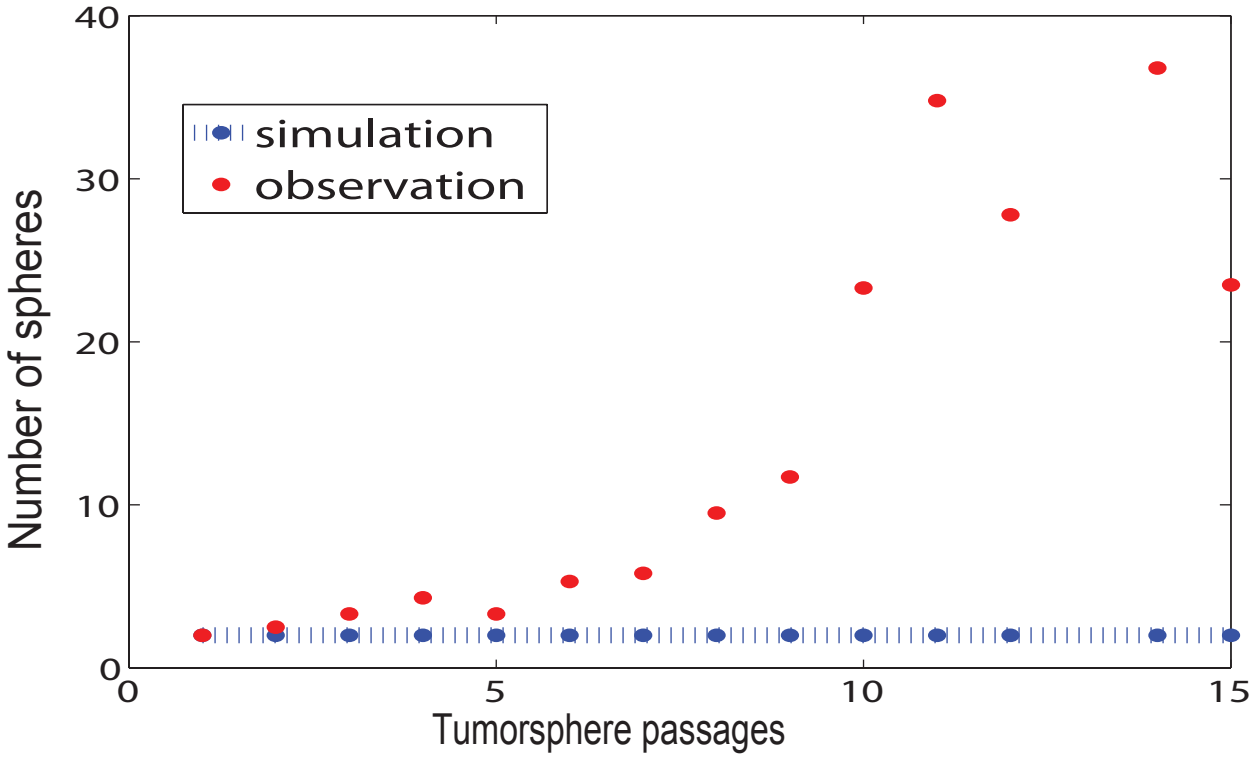
simulation
observation
Number of spheres
Tumorsphere passages
0
10
20
30
40
0
5
10
15

b.

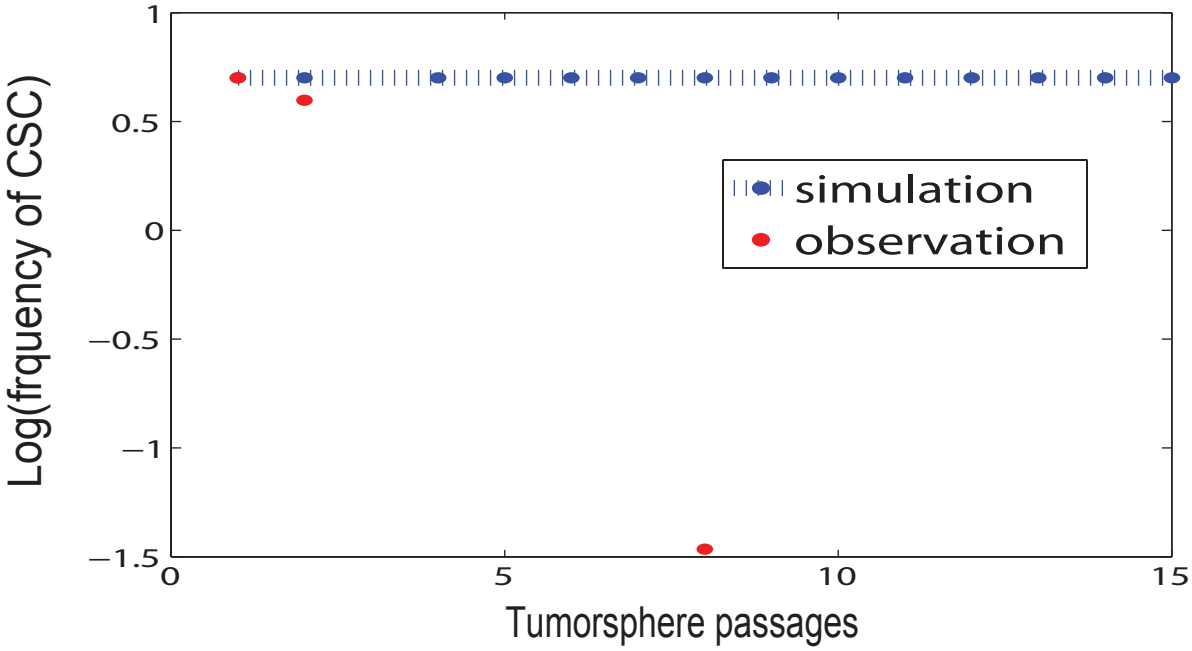
simulation
observation
Log(frquency of CSC)
Tumorsphere passages
1
0.5
0
−0.5
−1
−1.5
0
5
10
15

Fig. S8